# TECTONIC EVOLUTION OF THE IRRA PULL-APART BASIN EVIDENCES OF SLIP REVERSALS ON THE ROMERAL FAULT ZONE, NORTHERN PART OF ANDEAN CENTRAL CORDILLERA, COLOMBIA

# EVOLUCIÓN TECTÓNICA DE LA CUENCA DE TRACCIÓN IRRA. EVIDENCIAS DE CAMBIOS EN EL MOVIMIENTO DE RUMBO DE LA ZONA DE FALLA DE ROMERAL, ZONA NORTE DE LA CORDILLERA CENTRAL DE LOS ANDES, COLOMBIA.

G.M. SIERRA

*M.Sc. Department of Geology, University EAFIT, Colombia , gsierra@eafit.edu.co*

M.I. MARÍN-CERÓN

*PhD., Department of Geology, University EAFIT, Colombia*

W. MACDONALD

*Ph.D Department Geological Sciences, State University of New York at Binghamton, United States*

Recibido para evaluación: 30 Octubre 2012/Aceptación: 15 Noviembre: 2012 / Recibida Versión Final: 29 Noviembre 2012

**ABSTRACT:** The Irra Basin is a small pull-apart basin at the south end of North Cauca basin located between the Cauca and Romeral fault system, near their northern convergence in the Colombian Andes. The Irra Basin developed in the Late Tertiary time and records slip reversals on the Romeral fault zone. The basin is believed to have developed above a right step-over on the Romeral system during a right-lateral slip episode. It was subsequently deformed during a younger episode of left-lateral slip inducing the closure of the basin during. To analyze sediment dispersal flow patterns of into the Irra Basin, we used anisotropy of magnetic susceptibility as a proxy for sediment fabric. It was found that the magnetic 'fabric' impressed in these young terrestrial clastics is strongly correlated with the deformation (i.e. the structure), as well as with the sedimentary fabric. Therefore, the paleomagnetic remanence may record the identified rotational movements. In general, the sediments preserved a widespread overprint of low coercivity, with both normal and reversed polarities, superimposed on a high coercivity component also with both normal and reversed polarities. The tilt-test shows that the low coercivity component correspond to a post-folding magnetization. The declinations of the characteristic direction and of its secondary overprint are consistent with approximately 30º and 20º net clockwise rotations, respectively, although clearly rotations of opposite senses have occurred here according to the structural evidence. The younger overprint is consistent with a late episode of right-lateral slip. Present-day microseismic activity on the Romeral Fault Zone supports left-lateral slip. Collectively, the structural, magnetic and microseismicity data are consistent with four regimes of opposed lateral slip on the Romeral fault zone in this region during the Late Tertiary. Alternations of lateral slip are indicated, with right-lateral slip domination due to long-term northeastward convergence of the Nazca plate towards South America plate.

**Keywords:** Irra basin, North Andes, Cauca-Romeral fault system, ASM

**RESUMEN:** La cuenca de Irra es una cuenca de pull-apart entre los sistemas de falla del Cauca y Romeral. Esta cuenca se desarrolló en el Terciario Tardío y registra cambios cinemáticos significativos. Inicialmente fue afectada por un sistema de desplazamientos dextrales que fue reemplazado por una cinemática sinestral lo cual causa el cierre de la cuenca. Los resultados de anisotropía de susceptibilidad magnética en los sedimentos presenta una fabrica magnética correlacionable con la deformación y la seidmentación.

En general, los sedimentos conservan una sobreimpresión generalizada de baja coercitividad, con polaridad normal e invertida, superpuestas en un componente de alta coercitividad también con polaridades tanto normal e invertida. La prueba del basculamiento muestra que el componente de baja coercitividad corresponde a una magnetización posterior al plegamiento. Las declinaciones de la dirección y características de su sobreimpresión secundaria son consistentes con ca. 20°-30° de rotación horaria. La sobreimpresión más joven está asociado a un episodio dextral. La microsismicidad por el contrario refleja un tectónica sinestral. El conjunto de datos estructurales, magnéticos y la sismicidad son consistentes con cuatro regímenes cinemáticos en la zona de fallas Romeral durante el Terciario Tardío. Los

cambios en la cinemática del sistema de fallas de Romeral estaría relacionada con la convergente hacia el noreste de la Placa Nazca con relación a la Suramericana.

**Palabras claves:** Cuenca Irra, Norte de los Andes, sistema de fallas Cauca-Romeral, ASM

## 1. INTRODUCTION

Oriented samples from Irra Formation were taken to define the source areas and dispersal paths for the sediments. The *anisotropy of magnetic susceptibility* (AMS) has been used worldwide a proxy for flow fabrics in sediments (e.g. Galehouse, 1968; Hamilton and Rees, 1970), and it became evident that these relatively poorly consolidated sediments had magnetic 'fabrics' which showed clear overprints related to rock structure. In particular, the $K_1$ axes, which are usually aligned with the flow aces of deposition, used to be closely correlated with the folding axes (e.g. Borradaile, 1988; Hrouda, 1970; Kligfield et al., 1981). The $K_1$ axes are unsuited in this case for defining sedimentary flow directions. The combination of ASM technique together with the paleomagnetism study (remanence directions), its a useful tool to decipher structural and tectonic movements and rotations associated with the basin sediments

The study of the Irra Formation located along the inter-Andean valley in the Northern Andes of Colombia (Figure 1), is an ideal place to apply the above-mentioned techniques because: (1) The multiple deformations observed in the field work such as overthrust of the sediments over the Quaternary deposits (Sierra, 1994); (2) the special tectonic setting in this region related to the triple-junction of Nazca, Cocos and South American plates and the assemblage of Choco-Panama arc and (3) fault-boundary contacts with the Romeral-Cauca system. In this study, we wave also compared our results with the paleomagnetic results on the intrusive rocks associated to the Combia Formation, which intrudes the Amagá and Irra Basins along the North Cauca Basin (MacDonald, 1980).

Our initial objective in sampling the Irra Formation sediments and ash flow deposits was to interpret the orientation of the flow direction from the direction of elongation of the ellipsoid of the anisotropy of magnetic susceptibility (AMS) (e.g. Galehouse, 1968; Rees, 1965; Lee et al., 1990; MacDonald and Palmer, 1990). However, structural deformation can over-print a secondary fabric on rocks, which may partially or completely mask the AMS response of the primary depositional fabric. This effect has been evaluated as a possible way to estimate parameters of rock strain (deformation or compaction) from the shape of the AMS ellipsoid (*cf.* Kligfield et al., 1981; Lowrie and Hirt, 1987).

Experimentally, Richter et al. (1991) have shown in synthetic sediments that the AMS axes rotate away from the depositional fabric towards the deformational axes at strains exceeding 30%.

The focus of the present study is located at the south end of the North Cauca Basin just west of the Romeral fault. This region has been and remains very active tectonically. It lies approximately at the boundary between the accreted terrenes of oceanic materials and the ancient continental lithosphere (e.g. Cediel et al., 2003). It lies close to the Caribbean – South America – Nazca plate triple junction. And it marks approximately the northern limit of Latest Tertiary to present volcanism associated with subduction of the Nazca plate beneath the Andes. The movements described in this basin may provide an important discussion point related to the Andean Orogeny during the late Cenozoic.

So far, we hypothesized that the AMS signature of the Irra Formation might be useful for deciphering depositional flow paths, or alternatively for characterizing strain, thus we collected measurements to define both sediment flow directions and fold axial trends for comparison with the AMS. The gotten data indicates that the obliquely crossing the Irra Basin is NE-trending folds and thrust faults, thus we can interpret these as having formed by a reversal of the sense of slip along the boundary faults. This left-lateral movement attempted to close the Irra basin, and produced the folds and faults. Bedding poles define NE fold axis trends (azimuth 036º, plunge 01º). These structures are oblique to the dominantly NS trends of the Cauca and Romeral fault zones which bound the Cauca depression.

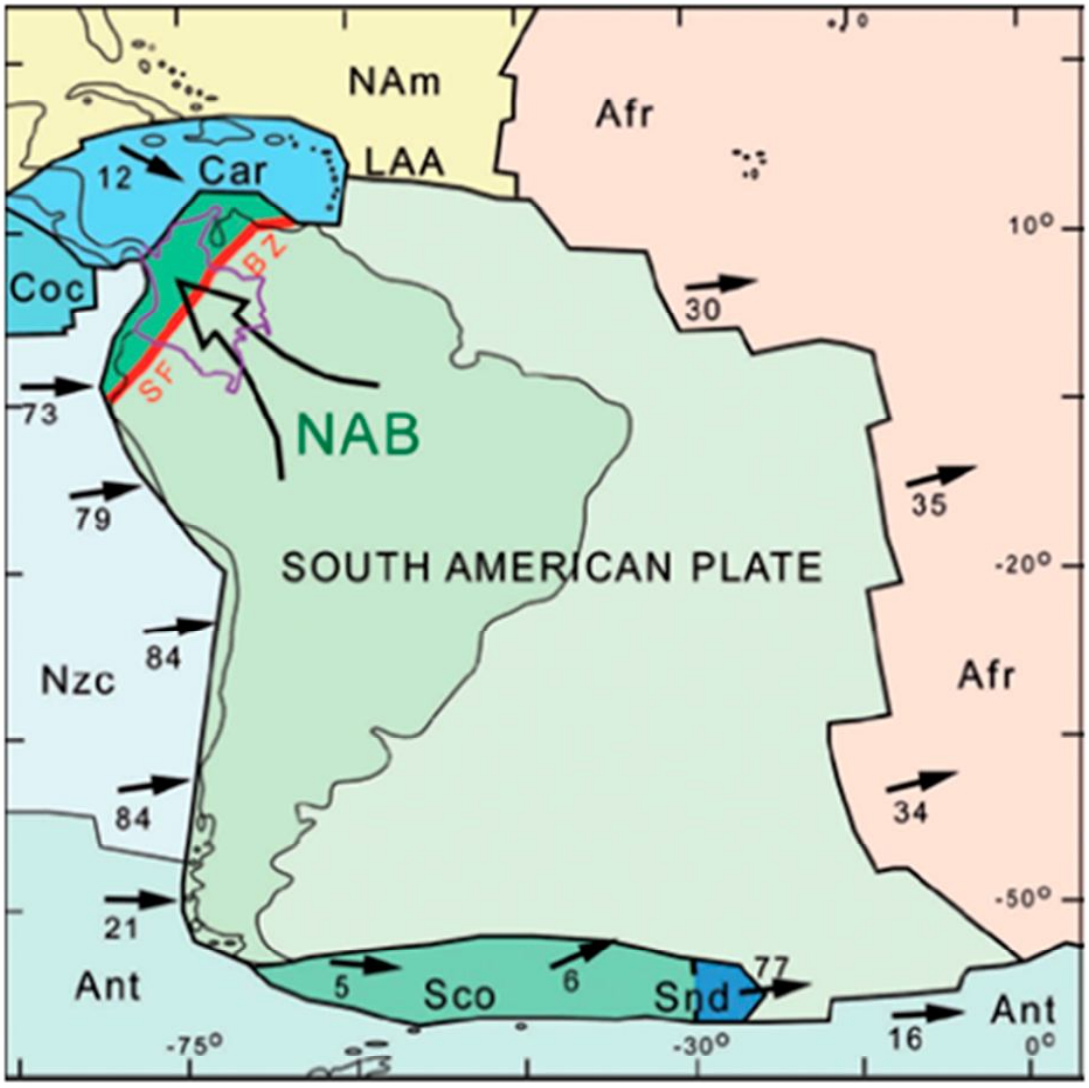


**Figure 1**. Regional tectonic setting of northwest South America. Striped pattern shows distribution of accretionary mainly Mesozoic terranes. Arrows show contemporary relative plate convergence directions and rates, rectangle locates area of index map to study area (modified from Cediel *et al*., 2003 in Sierra and Marín-Cerón, 2012 ). Key: NAB, North Andes Block; SFBZ, Stress Field Break Zone; Afr, African plate; Ant, Antartic plate; Car, Caribbean plate; Coc, Cocos plate; LAA, Lesser Antilles Arc; Nam, North American plate; Nzc, Nazca plate; Sco, Scotia plate; Snd, South Sandwich plate; SSA, South Sandwich Arc.

## 2. GEOLOGICAL SETTING

The Romeral fault zone (RFZ), which marks the approximate western limit of ancient South American lithosphere, is part of a major zone dominated by strike-slip faulting which stretches from the Peltetec fault of Ecuador (e.g. Litherland et al., 1993; Cediel et al., 2003) through most of Colombia (Fig. 1). Westward of Romeral-Peltetec fault zone lies a parallel fault zone, the Cauca-Pujilí fault zone, which similarly extends deep into Ecuador (Cediel et al., 2003). These fault zones converge in northern Colombia. In this region there accumulated up to several thousand meters of Tertiary terrestrial sediments (Grosse, 1926) in the North Cauca Basin, with some marine influence in the Amagá Formation (Sierra, et al submitted paper). These sediments have been deformed by Late Tertiary movements, and intruded by andesites and basalts dikes and sills associated to the Combia Volcanism (Figure 2).

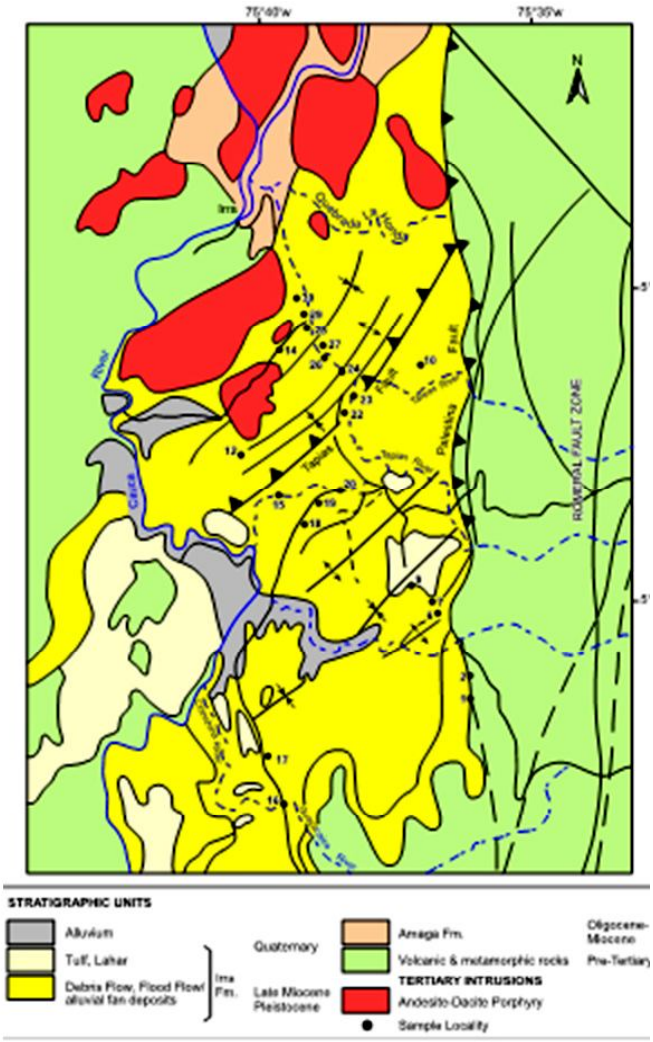


**Figure 2.** The late Tertiary Irra pull-apart basin is located adjacent to the Romeral fault zone, at the south end of North Cauca Basin. Sample localities for the rock magnetic studies are shown by numbered dots.

### 2.1. Stratigraphy and structure of the Irra basin

The Irra Basin is about 35 km long and 15 km wide. Its eastern boundary is marked by the Piedecuesta and other faults of the RFZ, which places sediments of the basin in contact with the Paleozoic and older crystalline rocks of the Cordillera Central (Figure 2). The western margin of the basin is generally faulted, but inactive at present. The locus of that fault is approximately along the Chinchiná-Cauca rivers zone west of which are exposed Cretaceous basaltic rocks correlative with the Barroso Formation.

The Late Tertiary sediments of the Irra Basin lies over older Tertiary strata and the deformed and accreted Cretaceous oceanic crustal rocks (Figure 2). The lowest part of the Tertiary section consists of sandstones, siltstones, and conglomerates, with minor beds of coal; these are thought to correlate with the upper part of the Amaga Formation (Grosse, 1926). Irra formation unconformably is referred informally as the above sequence with pyroclastic, epiclastic, and fluvial sediments (Sierra, 1994).

This formation was subdivided by Sierra (1994) into three informal members, A, B, and C. The lowest member C, exposed in the south half of the Irra Basin, contains debris flows (polymict conglomerates) interbedded with sandstones containing a small percent of reworked pyroclastic material. Member B, exposed in the north half of the basin, has been thrust southwards over member C along the Tapias thrust. Member B

contains hyperconcentrated flood-flow deposits of epiclastic origin (lapilli-volcanic conglomerate, tuff-sandstone) and minor ash flows .

Fission track dating of pink zircons from this member yields ages close to the Miocene-Pliocene limit (6.3±0.2, Toro et al., 1999). Member A, is unconformable above the lower units, and contains lahars, tuff, and related pyroclastic deposits. The Irra formation is believed to be Late Miocene to Pleistocene, and probably correlates in part with the upper part of the Combia Formation (e.g. Grosse, 1926; Sierra, 1994). Structural and sedimentary fabric component were measured by Sierra (1994) and they area summarized in Figure 3a-b.

Several small Late Tertiary hypabyssal intrusions occur in the northern part of the Irra Basin. These and similar intrusions elsewhere in the North Cauca Basin are 6 to 10 ma old (e.g. Restrepo et al., 1981, Jaramillo, 1981). The calc-alkaline geochemical signature of these intrusions (e.g. Jaramillo, 1981) indicates that those intrusions are related to the subduction-related magmatism along the Pacific margins of South America. The present axis of volcanism at this latitude now lies further east, approximately along the axis of the Cordillera Central, and suggests a change in subduction environment such as a shallowing of the slab angle in the past 6 to 10 ma.

In summary, the Irra Basin structural geology could be the result of the combined subsidence and uplift cycles that developed a number of sedimentary basins in the Cauca inter-Andean depression, which are limited by the Romeral and Cauca fault zone (Sierra, 1994).

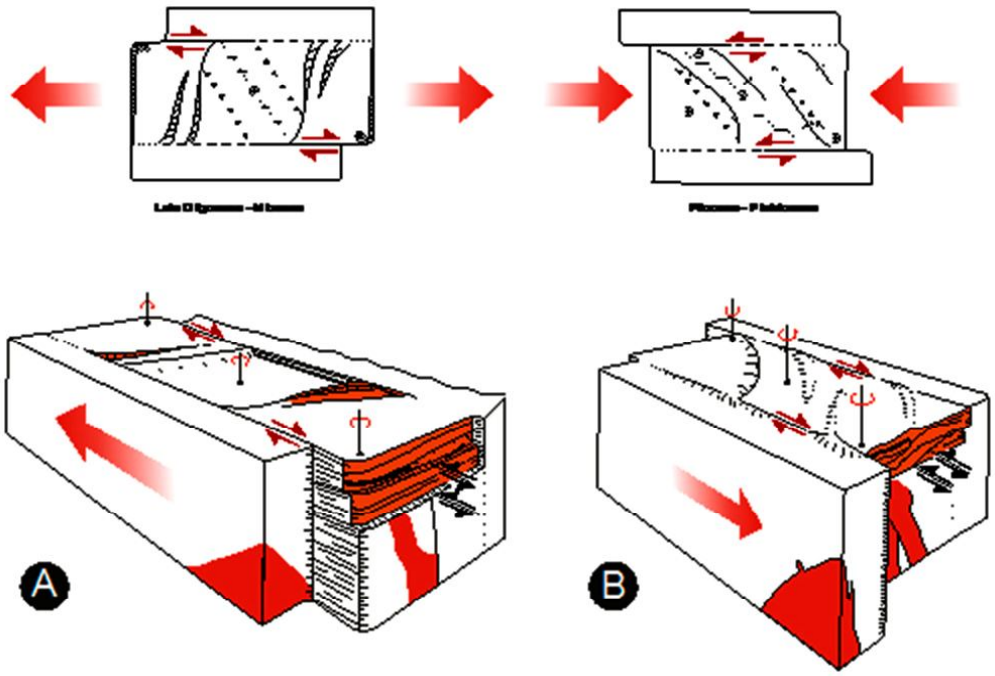


**Figure 3**. The development and deformation of the Irra Basin accompanied a reversal of slip along the Romeral fault zone. (A). Basin initiation and filling accompanied right-lateral slip above a right step-over now buried beneath the basin, as the west (left) block moved north relative to the east block. (B) Slip reversal, becoming left-lateral, compressed the strata in the Irra Basin, forming folds and thrusts, as the west block moved south relative to the east block. Counterclockwise rotations along stratal contacts probably accompanied the opening of the basin in right-lateral phase (A), and clockwise rotations accompanied compressions during the left-lateral phase (B) (modified from Sierra and Marín-Cerón, 2012).

## 3. METHODS

Field work sediments sampling in the Irra Basin were collected using oriented cubic plastic boxes (2 $cm^3$), following slot sampling method with a portable electric saw for unconsolidated sediments (Ellwood et al., 1993). Six samples per site were taken at 16 sites throughout the basin. AMS measurements were

performed using the KLY-2 Kappabridge instrument at Colgate University. Data were analyzed using Lienert's implementations of Hext/Jelinek statistical analysis (Lienert, 1991; Hext, 1963; Jelinek, 1978). The data was also re-analyzed at EAFIT University in the Paleomagnetism laboratory, using ANISOFT software.

## 4. RESULTS AND INTERPRETATIONS

### 4.1. Anisotropy of Magnetic Suceptibility (AMS)

#### 4.1.1. Results

The site-mean directions of the principal susceptibility axes are summarized in Table 1 (Figures 4- 6). Conventionally, the maximum, intermediate, and minimum axes of susceptibility are represented by $K_1$, $K_2$, and $K_3$, respectively. A relatively moderate anisotropy its observed, reaching about 3% in 'elongation' as represented by the ratio $K_1/K_2$, and about 7% of 'flattening' of the AMS ellipsoid as represented by the ratio $K_2/K_3$. These ratios show that the corresponding AMS ellipsoids for these mainly sedimentary rocks are slightly oblate, and somewhat less prolate than oblate.

The AMS axes and their means are plotted for each site. For most sites, the axes are well clustered, except for a few data in which $K_2$ and $K_3$ axes exhibit mixed populations. The $K_1$ axes-trend is dominantly NE/SW, with shallow inclinations, approximately parallel to the regional fold axis of the Irra Basin (*cf.* Figure 4a) rather than to the measured flow directions (Figure 4b). On the other hand, the $K_3$ poles show much more variability, from gentle to steep. Finally, the $K_3$ poles plot near the center of the stereoplot, are representing a near-horizontal 'flattening' planes for the corresponding AMS ellipsoid, therefore, those $K_3$ poles near the prime represent near-vertical 'flattening' planes.

**Table 1**. AMS Site-mean (*in situ*).

| Site | K | $K_1 / K_2$ | $K_2 / K_3$ | $K_1$ | | $K_2$ | | $K_3$ | |
|---|---|---|---|---|---|---|---|---|---|
| | | | | Dec | Inc | Dec | Inc | Dec | Inc |
| 9.3 | 10.3 | 1.102 | 1.064 | 105.5 | 15.8 | 354.5 | 51.1 | 026.7 | -34.5 |
| 10.2 | 7.6 | 1.026 | 1.022 | 355.1 | 51.8 | 021.6 | -35.2 | 102.2 | 13.1 |
| 12.5 | 9.4 | 1.010 | 1.016 | 223.9 | -06.1 | 300.5 | 65.4 | 316.6 | -23.7 |
| 16.1 | 14.0 | 1.017 | 1.037 | 031.0 | 44.8 | 136.5 | 15.2 | 060.3 | 41.3 |
| 16.5 | 8.5 | 1.030 | 1.030 | 046.2 | 51.3 | 321.4 | -04.1 | 234.6 | 38.4 |
| 19.1 | 6.7 | 1.022 | 1.024 | 0.56.3 | 42.0 | 125.4 | -21.6 | 015.8 | -40.2 |
| 24.1 | 7.5 | 1.012 | 1.029 | 013.9 | 55.6 | 092.5 | -07.7 | 357.4 | -33.3 |
| 26.3 | 6.1 | 1.013 | 1.021 | 037.0 | 11.0 | 204.1 | 78.7 | 306.6 | 02.5 |
| 27.6 | 3.9 | 1.080 | 1.016 | 040.1 | 11.1 | 202.9 | 78.4 | 309.5 | 03.3 |
| 27.7 | 8.1 | 1.008 | 1.014 | 020.4 | 17.8 | 168.1 | 69.2 | 107.0 | -10.4 |
| 28.A | 7.3 | 1.005 | 1.018 | 046.8 | -17.9 | 332.5 | 40.0 | 118.3 | 44.6 |
| 28.B | 4.5 | 1.034 | 1.023 | 064.7 | -28.5 | 332.1 | -04.9 | 053.2 | 61.0 |
| 29.6 | 10.5 | 1.026 | 1.054 | 023.2 | -00.2 | 48.0 | 087.8 | 087.8 | 87.8 |
| 30.2 | 3.3 | 1.013 | 1.084 | 065.0 | -16.6 | 328.1 | -22.0 | 009.1 | 61.9 |
| 30.3 | 1.4 | 1.008 | 1.005 | 110.4 | 10.4 | 021.6 | -06.1 | 321.8 | 77.9 |
| 31.1 | 15.7 | 1.022 | 1.061 | 006.3 | -00.5 | 276.4 | 38.0 | 089.5 | 86.2 |

K is site-mean volume susceptibility x $10^{-3}$ SI units; $K= (K_1+K_2+K_3) / 3$

$K_1$, $K_2$, and $K_3$ are axes of maximum, intermediate, and minimum susceptibility

D and I are declination and inclination in degrees

$K_1/K_2$ and $K_2/K_3$ are ratios of susceptibilities

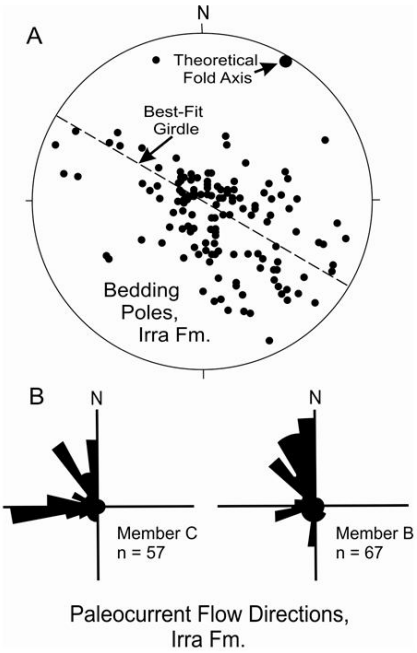


**Figure 4** . Structural and sedimentary fabric component for comparison with axes of anisotropic susceptibility. A) Bedding poles, Irra Formation, have mainly gentle dips. Least-squares fit provides a theoretical girdle representing folding about a theoretical fold axis plunging 01º towards N31E. B) Paleocurrent flow directions for the Irra Formation indicate flows directions, bimodal N and W in the lowest member C and unimodal N is member B (modified from Sierra and Marín-Cerón, 2012).

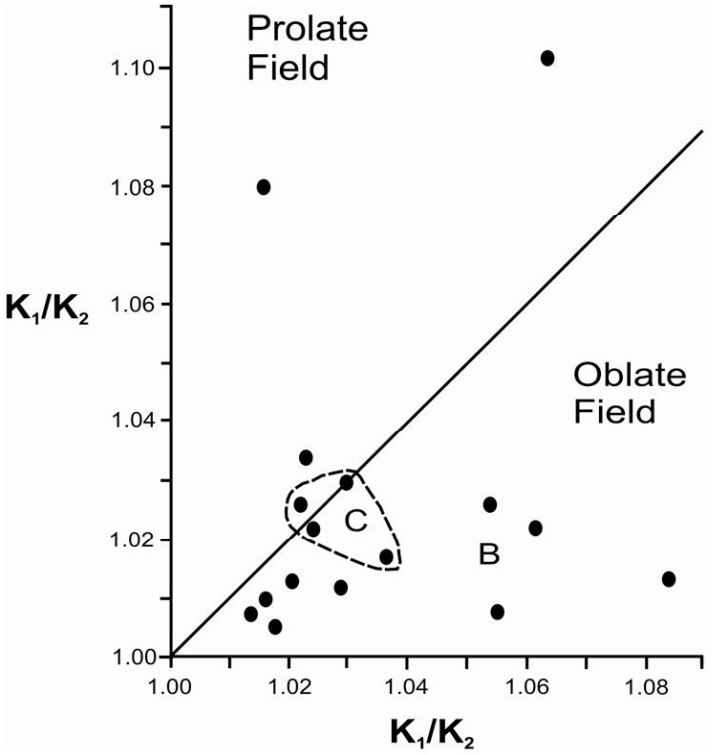


**Figure 5**. The axial ratio plot of site-means for the anisotropy of magnetic susceptibility (AMS) shows that elongation ($K_1/K_2$), of up to about 3%, is exceeded by flattening ($K_2/K_3$), of up to 7%. B and C refer to members B and C of the Irra Formation.

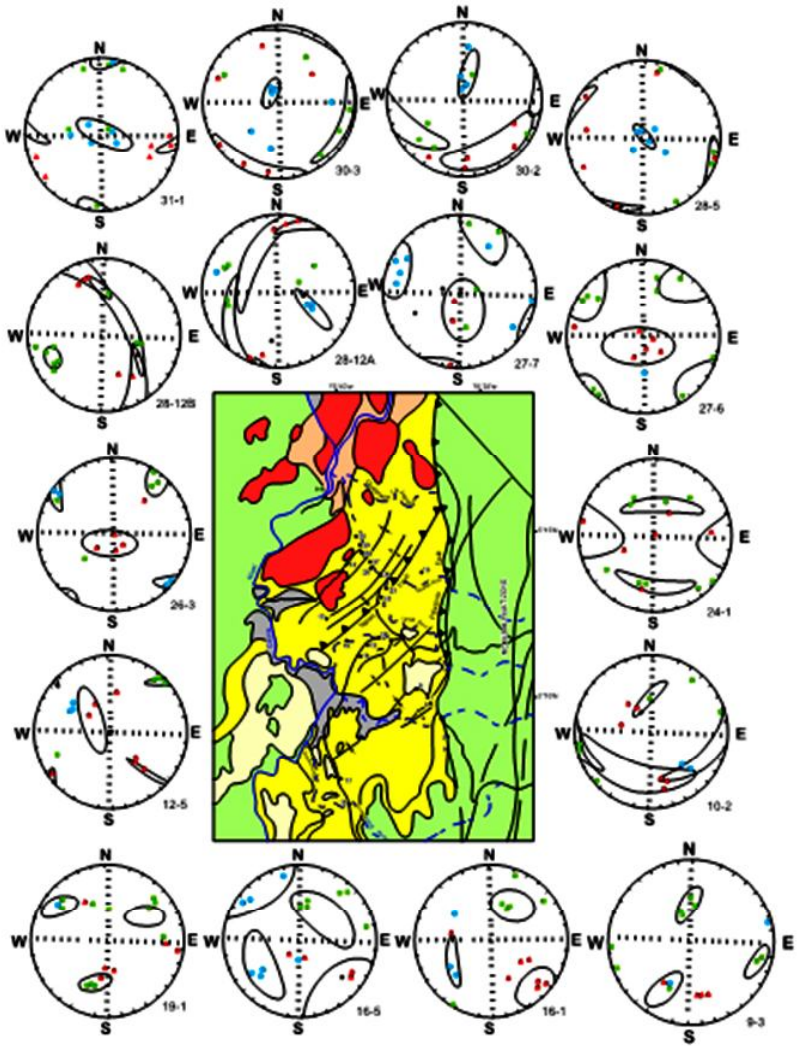

**Figure 6**. Site-means AMS results for the Irra Basin show good correspondence with the structural features. The $K_1$ (maximum susceptibility) axes are mainly oriented NE/SW parallel to the regional fold trends of the basin, and the $K_3$ (minimum susceptibility) axes lie mainly along the bedding girdle (*cf.* Figure 3), or are near the expected pole of the near-vertical fold-axis surface. Squares, triangles and circles represent the $K_1$, $K_2$, and $K_3$ axes, respectively. Lower hemisphere, equal area projection.

### 4.1.2. Interpretation

To clarify the individual patterns of the $K_1$ and $K_3$ axes, their site-means are plotted separately in Figure 6. The $K_1$ axes clearly trend mainly NE/SW (Figure 7a). There are two 'outliers', for site 9.3 and 30.3, with ESE trends, possibly representing primary flow fabrics. The mean for all $K_1$ axes plunges 17º towards azimuth 040º. Excluding the two outliers, the $K_1$ axial mean (14 sites) plunges 17º towards azimuth 035º. This compares favorably with the mean fold axis determined by eigenvalue methods from the individual bedding poles, which gives a mean fold axis plunging 01º towards azimuth 036º. The mean fold axis for the 12 *localities* represented by the 16 sampling sites yields a mean plunge of 04º towards azimuth 051º. The latter is less representative of the regional structural variations than is, for example, the larger data set of Figure 7a. Field measurements of sedimentary flow indicators (Figure 7b) indicate a unimodal northward flow in member B, and a bimodal northward and westward flow in member C.

The $K_1$ axes clearly correlate better with the fold axes than with the sedimentary flow axes. The implication of the $K_1$ axial distributions is that they represent

primarily strain effects, and do not indicate depositional flow fabrics. Putting it another way, although visually the obvious fabric in these rocks is depositional rather than deformational, the AMS 'fabrics' see the situation in opposite way, with deformation dominating depositional effects insofar as the $K_1$ axes are concerned.

In Figure 7b, the $K_3$ site-mean axes define a girdle not unlike that defined by the bedding poles, except that some $K_3$ lie near the prime. The latter clearly represent poles to near-vertical axial planes. Curiously enough, the latter are all in relatively massive ashflows, for which the AMS $K_3$-axes suggest that deformational fabrics dominate over depositional fabrics for both the $K_1$ and $K_2$ - axes.

Spatial variability of the AMS susceptibilities occurs within the Irra Formation at each member. Because there is only one site (no. 12.5) in member A, we can mainly discount that member. The axial ratios for member C sites cluster close together (dashed line, Figure 5). Also, the $K_1$ axes for member C tend to plunge more steeply (Figure 7a), and the $K_3$ poles are correspondingly displaced (Figure 7b). All sites for member C are located in the south half of the Irra Basin.

The AMS ash-flow fabric is clearly different from that of the enclosing sediments. These isolated ashflows, in member B, have well-grouped $K_1$ axes near the fold-axis trend (Figure 7a). $K_3$ poles for the gently-dipping ashflows indicate steeply-dipping planes of ellipsoid flattening (Figure 7b). Apparently the magnetic fabric of these competent ashflows records the strain effects associated with folding better than do the fabrics of the less competent sediments. This unusual result seems counter-intuitive; therefore further study in this and other settings is much needed.

In sum, the $K_1$ axes tend to replicate structural fold axial trends, whereas the $K_3$ axes are mainly expressing bedding pole trends, the few exceptions in the ashflows reflecting fold axial surfaces.

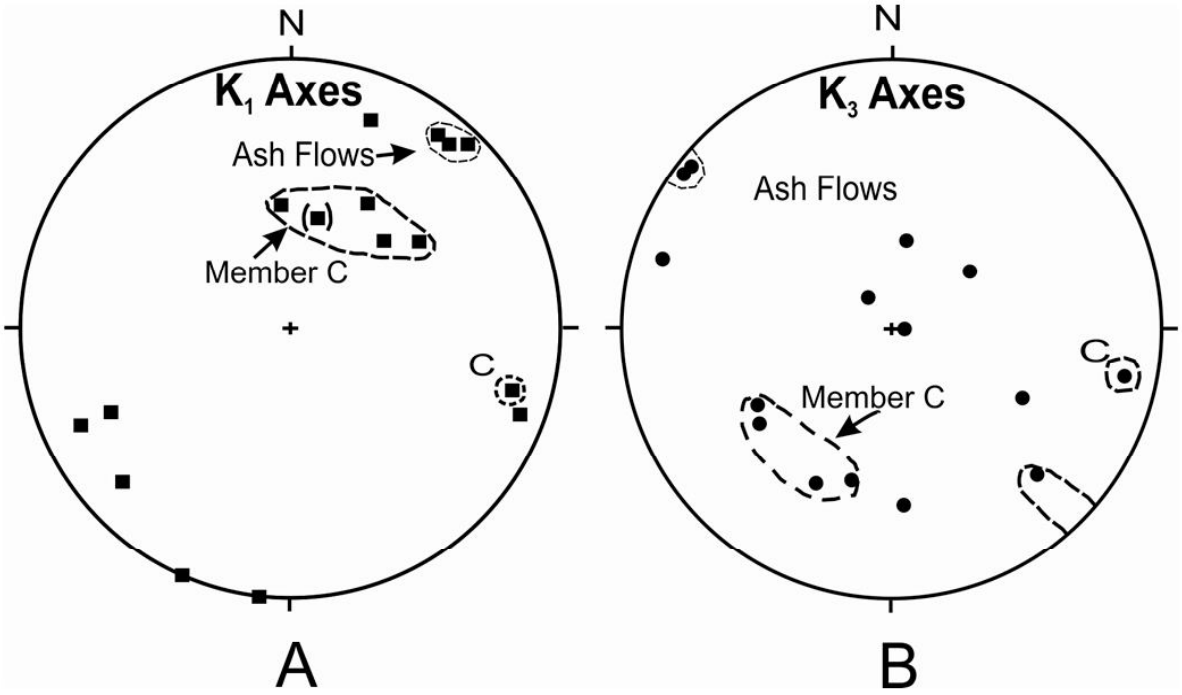


**Figure 7**. Site-mean principal susceptibility axes plotted separately. A) $K_1$ axes trend NE/SW parallel to the fold axes of the Irra Formation. Ashflow axes group well and are distinct from AMS axes for sediments. Axes for member C plot in distinct group. B) $K_3$ axes define a girdle about NE-trending fold axes. $K_3$ poles near the center of the stereoplot have shallow dips for the ellipsoid flattening, indicating that primary (i.e. sedimentary) parameters dominate. $K_3$ poles at the NW edge of the plot suggest that secondary structural parameters (i.e. axial plane cleavage) influences the magnetic fabrics, and affects the ashflows more than the sediments.

### 4.2. Magnetic remanence (mr)

#### 4.2.1. Principles and applications

Paleomagnetic methods have long been used for many geologic applications, such as correlation, evaluation of structural rotation, allochthonous terrane displacement, and continental paleogeographic reconstructions (e.g. Irving, 1964; McElhinny, 1973; Valencio, 1980; Kissel and Laj, 1988; Butler, 1992; VanderVoo, 1993). Paleomagnetic measurements in the present study were made on the same samples used for AMS analysis with the objective of obtaining into structural rotations, which might have accompanied the deformation of the Irra Basin sediments. It was also desired to see if these sediments are suitable for magnetostratigraphic studies.

The friable condition of these samples required encapsulation in plastic boxes in order to work with them. Unfortunately, plastic encapsulation made the samples unsuitable for thermal demagnetization. Therefore, the demagnetization studies were limited to a.f. demagnetization. The samples were measured and a.f. demagnetized using the 2G cryogenic magnetometer and automatic degaussing equipment at the University of Pittsburgh. The remanence components were evaluated using principal components analysis. The a.f. Demagnetization was carried out at multiple steps up to 90 mT, a typical sequence being 0, 2, 10, 12, 14, 20, 25, 35, 45, 60, 70 mT peak fields. Usually upon reaching the 10 to 14 mT level, about 60% of the remanence intensity had been removed. The major part of the remanence intensity was carried by the lower coercivity components.

#### 4.2.2. Results

A rather surprising result of this study is the good grouping, in antipodal clusters, of the natural remanent magnetization (NRM) (Table 2). The NRM intensities are mainly on the order of 4 to 8 mA $m^{-1}$.

Most samples have two clearly defined components, a lower coercivity component 'A' that is easily isolated by principal components analysis (PCA), and a higher coercivity characteristic component 'B' which is less well defined by PCA. Table 3 summarizes the site-means, formation means, and the associated Fisher (1953) statistics for these two components, with respect to *in situ* (geographic) and tilt-corrected ('stratigraphic') coordinate systems.

**Table 2.** Site-mean NRM directions.

| Site | Dip | Az | Lth | M | In Situ | | Tilt Corrected | | | | | |
|---|---|---|---|---|---|---|---|---|---|---|---|---|
| | | | | | Incl. | Decl. | Incl. | Decl. | n. | R | κ | $\alpha_{95}$ |
| 9.3 | 19 | 141 | cs | C | 16 | 011 | 28 | 017 | 6 | 5.99 | 43 | 10 |
| 10.2 | 13 | 173 | cs | C | 06 | 209 | -04 | 209 | 6 | 4.3 | 3 | 47 |
| 12.5 | 25 | 011 | af | A | -10 | 198 | 15 | 198 | 5 | 5.8 | 21 | 15 |
| 16.1 | 07 | 132 | ms | C | -19 | 043 | -19 | 040 | 6 | 4.0 | 3 | 54 |
| 16.5 | 07 | 132 | ms | C | -19 | 043 | -10 | 040 | 6 | 4.0 | 3 | 54 |
| 19.1 | 12 | 306 | fs | C | -03 | 183 | 03 | 183 | 6 | 5.0 | 5 | 33 |
| 24.1 | 16 | 090 | cs | B | 06 | 003 | -12 | 004 | 6 | 3.7 | 3 | 51 |
| 26.3 | 24 | 087 | af | B | -05 | 021 | -27 | 024 | 5 | 4.9 | 156 | 6 |
| 27.6 | 58 | 319 | af | B | -17 | 212 | 05 | 206 | 6 | 4.8 | 4 | 37 |
| 27.7 | 58 | 319 | cs | B | -21 | 219 | -04 | 207 | 6 | 5.7 | 15 | 18 |
| 28.A | 58 | 330 | cs | B | -12 | 142 | 28 | 142 | 6 | 4.4 | 3 | 46 |
| 28.B | 58 | 330 | cs | B | 01 | 182 | 47 | 201 | 6 | 5.5 | 10 | 23 |

| Site | Dip | Az | Lth | M | In Situ | | Tilt Corrected | | | | | |
|---|---|---|---|---|---|---|---|---|---|---|---|---|
| | | | | | Incl. | Decl. | Incl. | Decl. | n. | R | κ | $\alpha_{95}$ |
| 29.6 | 53 | 070 | cs | B | -05 | 023 | -01 | 026 | 6 | 5.9 | 37 | 11 |
| 30.2 | 28 | 075 | ms | B | -26 | 164 | 03 | 164 | 6 | 5.9 | 36 | 11 |
| 30.3 | 28 | 075 | cs | B | -03 | 187 | 23 | 189 | 6 | 5.9 | 84 | 7 |
| 31.1 | 50 | 172 | cs | B | 11 | 046 | 35 | 067 | 6 | 5.6 | 13 | 19 |

NRM = natural remanent magnetization; Dip = bedding dip; Az = dip direction; Lth = lithology; cs, ms, and fs are coarse, medium, and fine sandstone; af = ash – flow; M = member; A, B, and C refer to member A, B, and ; Inc = inclination; Dec = declination; n = no, of samples; R, κ, and $\alpha_{95}$ are Fisher (1953) parameters.

**Table 3.** Paleomagnetic Components A and B.

| Site | Component A | | | | | | | Component B | | | | | | |
|---|---|---|---|---|---|---|---|---|---|---|---|---|---|---|
| | In Situ | | Tilt Corrected | | | | | In Situ | | Tilt Corrected | | | | |
| | Incl | Decl | Incl | Decl | n | κ | $\alpha_{95}$ | Incl | Decl | Incl | Decl | n | κ | $\alpha_{95}$ |
| 9.3 | 24 | 002 | 38 | 011 | 4 | 190 | 7 | | | | | | | |
| 12.5 | -03 | 200 | 21 | 202 | 5 | 14 | 19 | | | | | | | |
| 16.1 | -02 | 215 | -03 | 215 | 5 | 17 | 17 | 24 | 061 | 22 | 064 | 3 | 10 | 33 |
| 16.5 | | | | | | | | -08 | 035 | -07 | 034 | 3 | 10 | 34 |
| 19.1 | 07 | 167 | 16 | 169 | 5 | 55 | 9 | | | | | | | |
| 26.3 | -03 | 022 | -25 | 025 | 5 | 142 | 6 | | | | | | | |
| 27.6 | -03 | 208 | 16 | 215 | 5 | 8 | 25 | | | | | | | |
| 27.7 | -20 | 230 | -11 | 213 | 6 | 19 | 14 | | | | | | | |
| 28.A | -61 | 170 | -04 | 160 | 5 | 16 | 18 | 63 | 027 | 15 | 353 | 6 | 14 | 17 |
| 28.B | 09 | 190 | 46 | 218 | 4 | 49 | 12 | 42 | 068 | 26 | 025 | 4 | 8 | 29 |
| 29.6 | 08 | 030 | 13 | 019 | 5 | 22 | 15 | 00 | 228 | -22 | 218 | 3 | 8 | 29 |
| 30.2 | -31 | 164 | -03 | 165 | 5 | 314 | 4 | 21 | 006 | -06 | 005 | 6 | 120 | 6 |
| 30.3 | -01 | 189 | 24 | 191 | 4 | 15 | 21 | | | | | | | |
| 31.1 | 07 | 056 | 24 | 070 | 4 | 91 | 8 | 14 | 223 | -18 | 224 | 4 | 31 | 14 |
| mean 1 | 11 | 019 | | | 13 | 8.2 | 15 | | | | | | | |
| mean 2 | | | -04 | 019 | 13 | 6.1 | 18 | | | | | | | |
| mean 3 | | | | | | | | 23 | 042 | | | 7 | 7.2 | 24 |
| mean 4 | | | | | | | | | | 14 | 029 | 7 | 9.3 | 21 |

Sites 10.2 and 24.1 did not yield usable results. Inc = inclination; Dec = declination; n = no, of samples; R, κ, and $\alpha_{95}$ are Fisher (1953) parameters.

### 4.2.3. Interpretation

At least two different episodes of magnetizations can be identified. Moreover, is possible to determine that both episodes encompassed time long-enough to straddle at least one reversal. Unfortunately, at the moment we do not have any continuous stratigraphic sequence to evaluate the number of reversals present, but the results show that such and undertaking, i.e. defining the magnetostratigraphy for these strata, should be

feasible. Thus, to the future, the problem of thermal demagnetization of these friable materials however needs to be solved.

Basically we have secondary A components of lower coercivity, with normal and reversed polarities, superimposed upon higher coercivity characteristic B components, also with both normal and reversed polarities. For example, the NRM directions for an evidently normal site (site 9.3, Figure 8a) can be seen, upon demagnetization, to retreat through the origin into the opposites quadrants, suggesting a lower coercivity normal component superimposed on a higher coercivity reversed component (Figure 8c). Similarly, the reversed NRM directions of site 30.2 (Figure 8b) are seen upon demagnetization to have a lower coercivity reversed component superimposed on a higher coercivity normal component (Figure 8d).

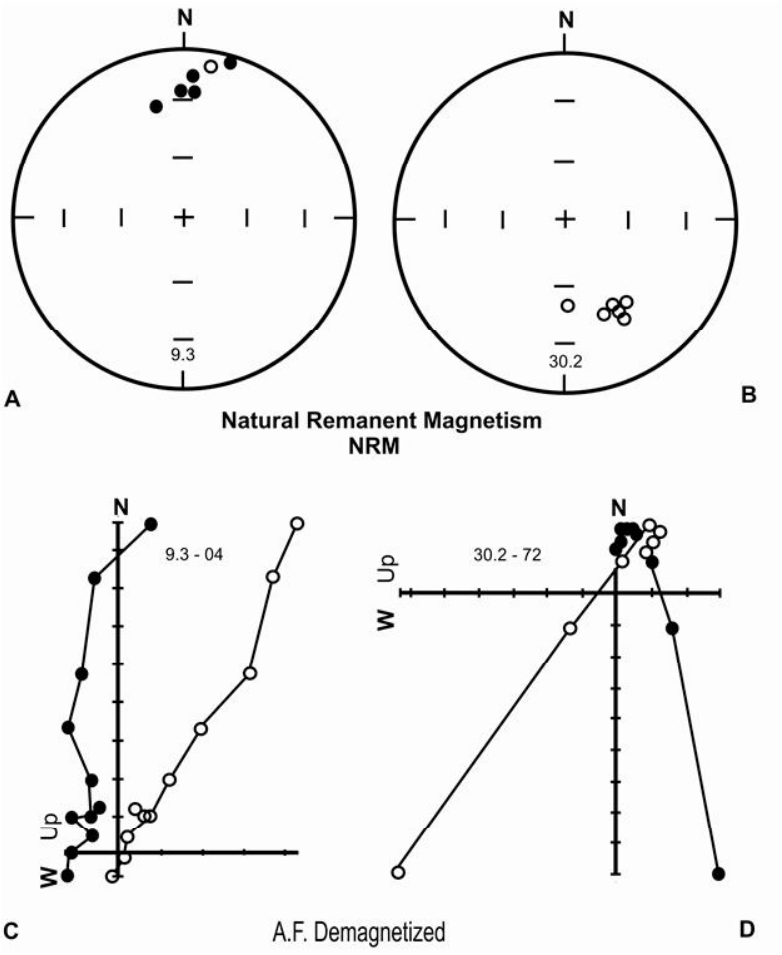


**Figure 8**. Examples of natural remanent magnetization (NRM) of the Irra Formation fall into two main groups of normal (A) and reversed (B) polarity. Both NRM populations have good within site clustering. (C) Zijderveld plot of the a.f. demagnetized components indicate that the high-coercivity characteristic component of (A) has reversed polarity, and (D) the high-coercivity characteristic component of (B) has normal polarity.

Examples of normal lower coercivity components superimposed on normal polarity higher coercivity components are found at site 26.3 (Figure 9a), and of reversed lower coercivity components superimposed on reversed higher coercivity components are found at site 20.7 (Figure 9a).

Although it was possible to derive well-defined lower coercivity components for 15 sites (Figure 10a, b), the higher coercivity components could not be so well isolated. What generally happened is that at higher demagnetization fields, the higher coercivity

component tended to acquire some treatment 'noise' (Figure 9c). Thermal demagnetization of the higher coercivity component, probably carried by hematite, is desirable but was not possible because of the friable plastic-encapsulated character of the samples. In the absence of thermal demagnetization, these higher coercivity components could not be precisely resolved. The result is that higher coercivity components with reasonably acceptable Fisher statistics were obtained at only 7 of the 15 sites (Figure 10c, d; Table 3).

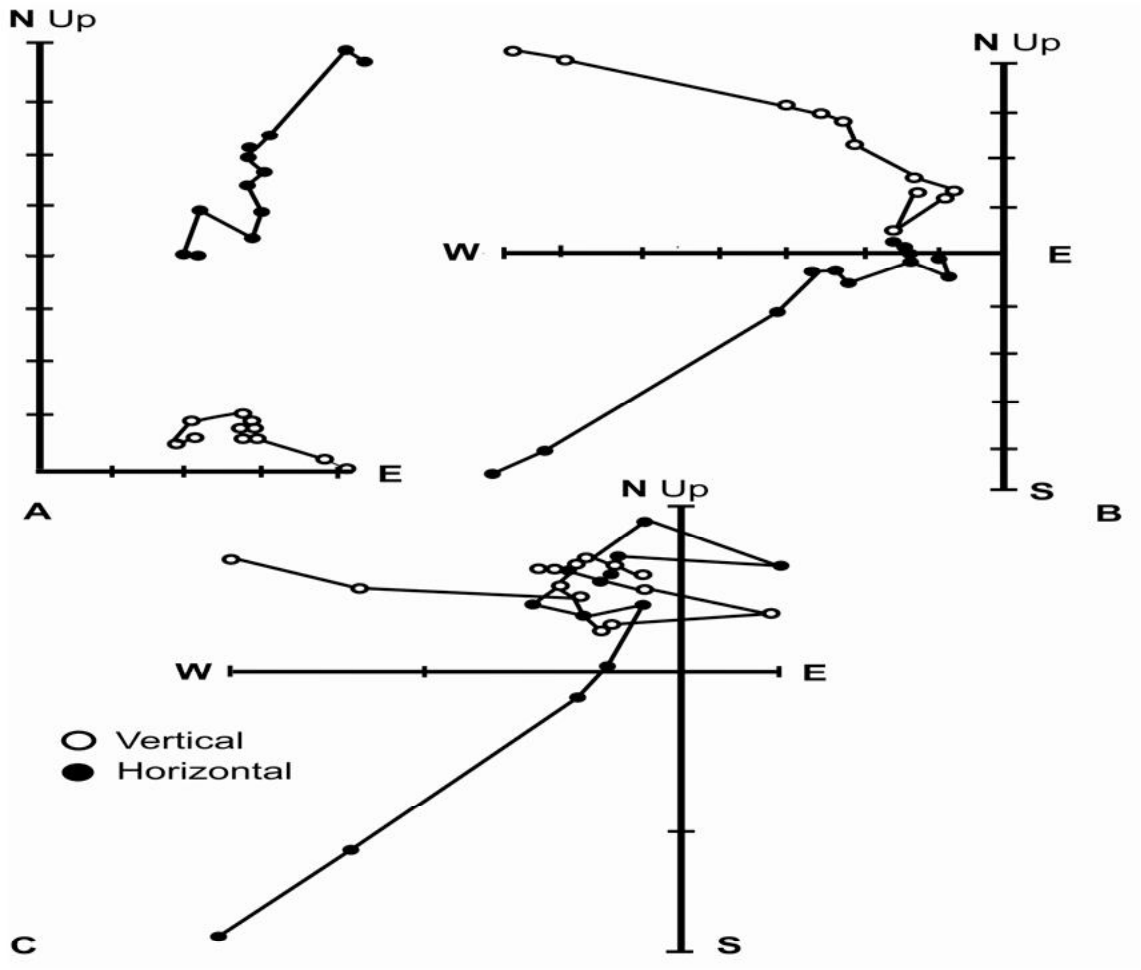


**Figure 9. A**) Examples of Zijderveld vector orthogonal plots of a.f. demagnetization results for sites which show a normal low coercivity component overprinting a higher coercivity component also of normal polarity, and the higher coercivity component is well defined. B) Similar to (A), except that the lower and higher coercivity components are both of reversed polarity. C) For many sites, progressive a.f. demagnetization reveals a well-defined lower coercivity component, but at higher peak fields is unable precisely to isolate the higher coercivity component. Marks on axes at 25 x $10^{-5}$ emu intervals.

From its lower coercivity in a.f. demagnetization, it seems probable that component A resides in magnetite or maghemite. The higher coercivity component B is possibly carried by hematite as well as by magnetite, as some directions change very little under a.f. demagnetization, even up to 90 mT.

Both the lower coercivity and higher coercivity components show antipodal reversals. However, the *dominant* polarity for the lower coercivity component A is *reversed*, and the *dominant* polarity for the higher coercivity components B is *normal* (Figure 10).

The tilt-correction was applied to both low coercivity and to high coercivity directions (Table 3 and Figure 10). It is found that the lower coercivity components are better grouped *in situ* (i.e. without the tilt correction), with corresponding kappa values of 8.2 *vs*. 6.1, without

and with tilt correction, respectively, for 13 sites. A small statistical improvement could be obtained by omitting outliers. The high-coercivity components B are better grouped with tilt correction than without. For the 7 sites for which component B was reasonably recoverable, the corresponding kappa values are 9.3 with tilt correction and 7.2 without tilt correction. These differences indicate that the lower coercivity component A was acquired *after* folding, and the higher coercivity component B was acquired *before* folding. We conclude that component B is older than component A, and possibly represents the primary remanence.

The mean declinations for these remanence populations are also revealing. The mean declination for the *in situ* lower coercivity component A is, for normal polarity mean, 019º, with inclination 11º (Table 3). The mean declination for the tilt-corrected higher coercivity component B is 029º, with a mean inclination of 14º. The expected theoretical dipole field direction at this latitude, for comparison, is D = 000º, I = 10º. Both generations of remanence have been rotated clockwise from north. The older component B has been rotated approximately 29º whereas the younger component A has been rotated about 19º. We surmise that these strata underwent a net clockwise rotation of 10º before they were remagnetized with component A. It is not clear if this 10º rotation took place before or after the folding, or if this is the net of two or more rotations predating component A (MacDonald, 1980). We can conclude that after the remagnetization, these strata were rotated clockwise approximately 19º (i.e., the observed declination minus the expected declination is 019º - 000º). Because clockwise rotations are consistent with right lateral slip, and because the folding probably occurred during left-lateral slip (Figure 3b), we propose that following the folding, another reversal of the slip-sense on the Romeral fault occurred, becoming again right lateral, and rotating component A clockwise to its present declination.

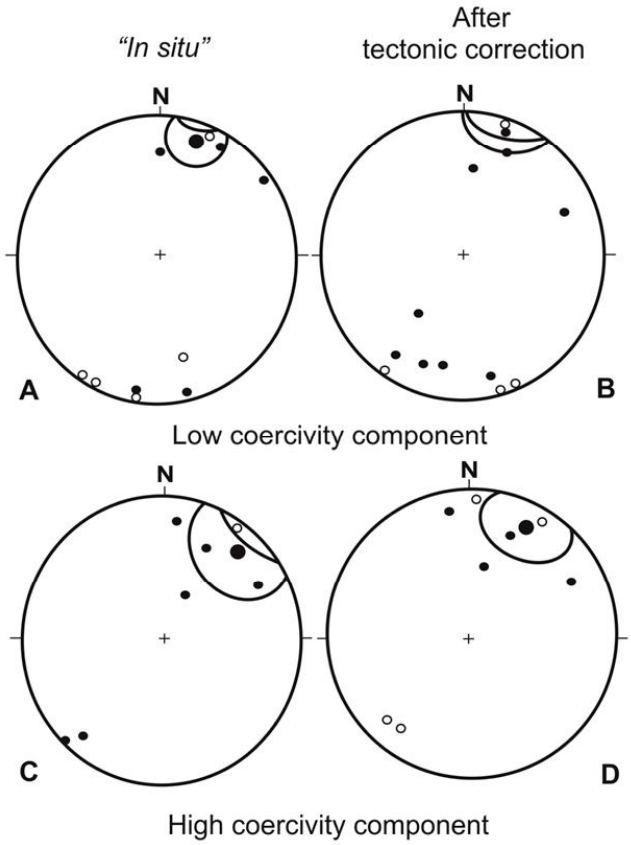


**Figure 10.** The lower *vs*. higher coercivity components (in rows) are compared in their *in situ* (geographic) *vs*. tilt-corrected (stratigraphic) orientations (in columns). The low coercivity components are better grouped before tilt correction (A) than after (B), whereas the higher coercivity components are better grouped after (D) than before (C) the application of the tilt correction. A to D correspond to means 1 to 4 in Table 3, respectively.

## 5. DISCUSSION ABOUT THE STRIKE-SLIP EPISODES OF THE ROMERAL FAULT ZONE

The development and deformation of the Irra Basin and its sediments point out, at least three episodes of strike-slip movement along the adjacent Romeral fault system; a fourth one may be indicated by present microseismic surveys. These are as follows:

I. Late Miocene event: an 'early' period of right lateral slip, during which the Irra pull-apart basin developed accompanied by some clockwise rotation of the early high coercivity component A in detachment sheets of Irra sediments (Figure 3a).

II. Pleistocene event: a middle period of left-lateral slip, during which the Irra basin was 'closed' with the accompaniment of compressive structures: folds and thrust-faults of NE trend; age: pre-dates the unconformity below member A, approximately; probably accompanied by counterclockwise rotation of component A on thrust faults (Figure 3b).

III. Late Pleistocene: a late period of right-lateral slip, during which the pre-folding and post-folding remanences of the Irra Basin were rotated about 20º clockwise; perhaps the same age as member A (Figure 10a).

IV. Holocene events: indicate left-lateral motion from microseismicity surveys (Hutchings et al., 1981) for the Romeral and Cauca fault systems.

The more easterly declination of the older B component (D = 029º) relative to the younger A component (D = 019º) seems a little unusual in view of our understanding of events, unless it was significantly rotated clockwise during phase *i* above. Otherwise, it would be expected to have a declination west of that of the younger component A, because phase *ii* would have rotated component B counterclockwise before the formation of component A which is post-folding, i.e. post-phase *ii*. The 20º rotations subsequent to the formation of component A affected both components A and B equally.

Finally, these results help to explain why both left-lateral and right-lateral slip have been reported for the Romeral and associated faults (Campbell, 1974; Hutchings et al., 1981; Dengo, 1985; Restrepo and Toussaint, 1988). Therefore, here after, it is not a question of *either* right- or left lateral, but rather a question of which sense of slip, at which locality and at what time.

Collectively the structural, paleomagnetic, and microseismic evidence indicate several alternations of slip-sense along the Romeral fault system since the Late Miocene. Presumably the long-term slip on the Romeral and associated continental-margin-parallel fault systems of Colombia and Ecuador is right lateral, consistent with the coast-parallel component of Nazca motion relative to the South American plate (Pardo-Casas and Molnar, 1987).

## 6. CONCLUSIONS

Three phases of strike-slip faulting along the Romeral fault zone can be deduced from 1) the formation of the Irra Basin, 2) the deformation of its sediments, and 3) rotation of its remagnetized sediments. The corresponding ages and slip-sense of these phases are i) Late Miocene right-lateral (syndepositional); ii) approximately Pleistocene left-lateral (syndeformational); iii) Pleistocene-Recent right-lateral (rotation of the remagnetized Irra Formation). An additional phase, iv) of left-lateral present-day slip has been deduced from microseismicity activity (Hutchings et al., 1981).

The $K_1$ axes of the AMS fabrics obtained correspond to phase ii fold axes of the Irra Formation, whereas the $K_3$ axes correspond mainly to phase i bedding poles; to a minor extent some $K_3$ poles correspond to vertical axial planes of phase ii folds, consistent with the overprint of sedimentary fabric by the structural AMS fabric. Two components of magnetization are present in these sediments. The older component B, of higher coercivity, was acquired pre-folding and probably dates from phase i; it has both normal and reversed polarities, and its mean direction is D = 029º, I = 14º, $\alpha_{95}$ = 21, $\kappa$ = 9.3, n = 7. The younger component A, of lower coercivity, has also both normal and reversed polarities overprinting component B, and is post-folding. Its age lies between the phase iii age of its rotation and the phase ii folding which preceded it. Its mean is D = 019º, I = 11º, $\alpha_{95}$ = 15º, $\kappa$ = 8.2, n =

13. The difference between the expected and observed declinations for the young component A (D = 000º *vs.* D = 019º, respectively) indicates approximately 19º of clockwise rotation for the Irra Basin sediments since approximately Pleistocene time. For the older component B, a net rotation of approximately 29º clockwise since Late Miocene is indicated.

## ACKNOWLEDGMENTS

Special thanks to Dr. Marthin Chadima, from AGICO Company for his continue support in the data process. This study was supported by ANH-Colciencias-EAFIT project (2009-2012) and the Laboratory Geosciences National Network (RNLG).

## REFERENCES

[1] Borradaile, G.J., 1988. Magnetic susceptibility, petrofabrics, and strain. Tectonophysics, **156**, 1 – 20.

[2] Butler, R.F., 1992. Paleomagnetism. Blackwell Scientific Publications, Boston, 319 p.

[3] Campbell, C., 1974. Colombian Andes *in* Spencer, A.M., editor. Mesozoic-Cenozoic Orogenic Belts. Geological Society of London, Special Publication, **14**, 705 – 724.

[4] Dengo, G., 1985. Mid-America; tectonic setting for the Pacific margin from southern Mexico to northwestern Colombia, *in* Nairn, A.E.M., Stehli, F.G., and Uyeda, S., editors. The Ocean Basins and Margins. Plenum Press, N.Y., **7A**, 123 – 180.

[5] Ellwood, B.B., MacDonald, W.D., and Wolf, J.A., 1993. The slot technique for rock magnetic sampling. Physics of the Earth and Planetary Interiors, **78**, 51 – 56.

[6] Fisher, R.A., 1953. Dispersion on a sphere. Proceedings, Royal Society of London, **A 217**, 295 – 305.

[7] Galehouse, J.S., 1968. Anisotropy of magnetic susceptibility as a paleocurrent indicator: a test of the method. Geological Society of America Bulletin, **79**, 387 – 390.

[8] Grosse, E., 1926. Estudio geológico del Terciario Carbonífero de Antioquia. D. Reimer, Berlin, 361p.

[9] Hamilton, N., and Rees, A.I., 1970. The use of magnetic fabric in paleocurrent estimation. In: *Paleogeophysics* (edited by S.K. Runcorn), 445 – 464, Academic Press, New York.

[10] Hext, G.R., 1963. the estimation of second-order tensors, with related tests and designs. Biometrika, **50**, 353 – 373.

[11] Hrouda, F., 1970. The relation between the fabric and anisotropy of magnetic susceptibility for some west Moravian gneisses. Czech. Ustred. Ustav. Geolo., Vestn, **45**, 147 – 156.

[12] Hutchings, L., Turcotte, T. McBride, J., and Ochoa, H., 1981. Microseismicity along and near the Dolores shear zone in Antioquia, Colombia. Revista, Centro Interamericano de Fotointerpretación, Bogotá, **6**, 243 – 256.

[13] Irving, E., 1964. Paleomagnetism and its applications to geological and geophysical problems. John Wiley and Sons, New York, 399 p.

[14] Jelinek, V., 1978. Statistical processing of anisotropy of magnetic susceptibility measured on groups of specimens. Studia Geophysicae et Geodeticae, **22**, 50 – 62.

[15] Kissel, K., and Laj, C., 1988. Paleomagnetic rotations and continental deformation. Kluwer Academic Publishers, Dordrecht, 516 p.

[16] Kligfield, R., Owens, W.H., and Lowrie, W., 1981. Mangetic susceptibility anisotropy, strain, and progressive deformation in Permian sediments from the Maritime Alps (France). Earth and Planetary Science Letters, **55**, 181 – 189.

[17] Lee, T. Kissel, C., Laj, C., Horning, C., and Lue, Y., 1990. Magnetic fabric analysis of the Plio-Pleistocene sedimentary formation of the Central Range of Taiwan. Earth and Planetary Science Letters, **98**, 23 – 32.

[18] Lienert, B. R., 1991. Monte Carlo simulation of error in the anisotropy of magnetic susceptibility: a second-rank symmetric tensor: Journal of Geophysical Research, **96**, 19539 – 19544.

[19] Litherland, M., Aspden, J. A., and Eguez, A., 1993. The geotectonic evolution of Ecuador in the Phanerozoic. Second International Symposium on Andean Geodynamics, Oxford University, Extended Abstracts. Editions de l'ORSTOM, L'Institut Francais de Recherche Scientifique pour le Developpement en Cooperation, Paris, 215 – 218.

[20] Lowrie, W., and Hirt, A. M., 1987. Anisotropy of magnetic susceptibility in the Scaglia Rosso pelagic limestone. Earth and Planetary Science Letters, **82**, 349 – 356.

[21] MacDonald, W. D., 1980. Anomalous paleomagnetic directions in Late Tertiary andesitic intrusions of the Cauca depression, Colombian Andes. Tectonophysics, **68**, 339 – 348.

[22] MacDonald, W. D., and Palmer, H. C., 1990. Flow directions in ash-flow tuffs: a comparison of geological and magnetic susceptibility measurements, Tshirege member (upper Bandelier Tuff), Valles caldera, New Mexico, USA. Bulletin of Volcanology, **53**, 45 – 59.

[23] McElhinny, M. W., 1973. Paleomagnetism and plate tectonics. Cambridge University Press, Cambridge, 358 p.

[24] Pardo-Casas, F. and Molnar, P., 1987. Relative motion of the Nazca (Farallon) and South American Plates since Late Cretaceous time. Tectonics, **6**, 233 – 248.

[25] Restrepo, J. J., and Toussaint, J. F., 1988. Terranes and continental accretion in the Colombian Andes. Episodes, **11**, 189 – 193.

[26] Restrepo, J. J., Toussaint, J. F., and Gonzales, H., 1981. Edades Mio-pliocenas del magmatismo asociado a la Formación Combia, departamentos de Antioquia y Caldas, Colombia. Geología Norandina, **3**, 21 – 26, Universidad Nacional de Colombia, Bogotá.

[27] Rees, A. I., 1965. The use of anisotropy of magnetic susceptibility in the estimation of sedimentary fabric. Sedimentology, **4**, 257 – 271.

[28] Richter, C., Frisch, W., Raschbacher, L., and Schwarz, H. U., 1991. The magnetic fabrics of experimentally deformed artificial clay-water dispersions. Tectonophysics, **200**, 143 – 155.

[29] Sierra, G. M., 1994. Structural and sedimentary evolution of the Irra Basin, northern Colombian Andes. Master thesis, Department of Geological Sciences, State University of New York, Binghamton, NY, 102 p.

[30] Valencio, D. A., 1980. El magnetismo de las rocas. Editorial Universitaria, Buenos Aires. 351 p.

[31] VanderVoo, R., 1993. Paleomagnetism of the Atlantic, Tethys, and Iapetus Oceans. Cambridge University Press, 411 p.